doi.org/10.36721/PJPS/2026.40.16635.1

A machine learning–based senescence scoring system reveals immunosuppressive tumor microenvironment remodeling and predicts prognosis in head and neck squamous cell carcinoma

Miaomiao Lu[1,2#], Yue Xi[4#], Yan Chen[1], Xinyu Liu[1,5], Ruiyu Guo[2], Qingqing Wan[2], Xin Zou[3*] and Wantao Chen[2,3*]

[1]College of Stomatology; Affiliated Stomatological Hospital, Binzhou Medical University, Yantai 264003, Shandong, China
[2]Department of Oral and Maxillofacial–Head and Neck Oncology; National Clinical Research Center for Oral Disease; Shanghai Laboratory of Stomatology; Shanghai Research Institute of Stomatology, Shanghai Ninth People's Hospital, Shanghai Jiao Tong University School of Medicine, Shanghai, China
[3]National Center for Translational Medicine (Shanghai), Linyi Branch; Institute of Translational Medicine, School of Medicine, Linyi University, Linyi 276000, Shandong, China
[4]Department of Obstetrics and Gynecology, Xinhua Hospital, Shanghai Jiao Tong University School of Medicine, Shanghai 200092, China
[5]Department of Stomatology, Shengli Oilfield Central Hospital, Dongying 257034, Shandong, China

Abstract: **Background**: Head and neck squamous cell carcinoma (HNSCC) exhibits pronounced molecular heterogeneity and limited durable response to immune checkpoint blockade (ICB). Cellular senescence is an emerging modulator of the tumor microenvironment, yet a validated senescence-based prognostic system for HNSCC remains lacking. **Objectives**: To develop and validate a senescence-based scoring system (SceScore) for predicting prognosis, characterizing immune microenvironment features and guiding therapeutic decision-making in HNSCC. **Methods**: Seven senescence- and metabolism-related gene sets were evaluated across 30 TCGA pan-cancer cohorts. Differentially expressed senescence genes in HNSCC were integrated using 101 machine learning algorithm combinations under a leave-one-out cross-validation (LOOCV) framework to construct SceScore. Prognostic performance was validated in three independent GEO cohorts (GSE42743, GSE65858, GSE41613). Associations with immune infiltration, drug sensitivity and tumor mutational burden (TMB) were systematically assessed. Single-cell and spatial transcriptomic datasets were analyzed to validate cellular origins and the spatial distribution of SceScore. **Results**: Senescence features showed the strongest pan-cancer association with survival and immune phenotypes. An eight-gene SceScore independently predicted overall survival across all HNSCC cohorts. High SceScore correlated with advanced stage, elevated TMB and an immunosuppressive microenvironment enriched for M0 macrophages and regulatory T cells, with upregulated PD-1/PD-L1, CTLA-4 and IDO1 expression. High-SceScore tumors exhibited reduced sensitivity to platinum-based chemotherapy but greater sensitivity to EGFR inhibitors. Single-cell analysis identified SPP1+ tumor-associated macrophages as the primary drivers of high SceScore and spatial transcriptomics confirmed their preferential enrichment at the tumor–stroma invasive front. **Conclusion**: SceScore is a robust, independently validated prognostic tool that captures senescence-driven immunosuppression in HNSCC, offering a clinically actionable framework for risk stratification and therapeutic decision-making, including guidance for ICB and targeted therapy selection.

Keywords: Cellular senescence; Head and neck squamous cell carcinoma; Immune checkpoint; Machine learning; Prognostic biomarker; Single-cell RNA sequencing; Spatial transcriptomics; Tumor microenvironment

Submitted 18-04-2026 – Revised 04-06-2026 – Accepted 14-07-2026

Article in Press

INTRODUCTION

Cancer remains a leading cause of morbidity and mortality worldwide, placing a substantial burden on global health systems (Sung *et al*., 2021). Head and neck squamous cell carcinoma (HNSCC) is the most common type of cancer, ranking sixth in global cancer incidence and accounting for roughly 5.3% of all new cases annually (Chaves *et al*., 2023; Gigot *et al*., 2022). Despite refinements in diagnostic imaging and the growing adoption of multimodal treatment protocols, locoregional recurrence and distant metastasis remain common and five-year overall survival rates have improved only modestly across most disease stages (Chow, 2020). The approval of pembrolizumab as a first-line agent targeting the PD-1/PD-L1 axis has reshaped the treatment landscape and opened new therapeutic possibilities (Ferris *et al*., 2016, 2018; Seiwert *et al*., 2016). Yet durable benefit from immune checkpoint blockade (ICB) is confined to a minority of patients. This reality reflects the deep molecular heterogeneity of HNSCC and the varied mechanisms through which tumors resist immune attack. Better tools for patient stratification are therefore an active clinical priority.

**Corresponding author:* e-mail: chenwantao196323@sjtu.edu.cn; albumxin@qq.com
#These authors contributed equally and are the co-first authors.

The tumor immune microenvironment (TME) is a key factor in the response to ICB in HNSCC. Tumors that fail to respond to checkpoint therapy often share a recognizable immune architecture: depleted cytotoxic CD8 T cells, expanded populations of regulatory T cells (Tregs) and tumor-associated macrophages (TAMs) and broad upregulation of inhibitory checkpoint molecule (H. Chen *et al*., 2022; Yang *et al*., 2024). Elevated tumor mutational burden (TMB) has been tied to improved neoantigen presentation and stronger immunotherapy responses in several cancer settings, yet how mutational load shapes the immune contexture in HNSCC specifically remains incompletely characterized (C. Zhang *et al*., 2022). Compounding this, the pronounced intratumoral heterogeneity of HNSCC makes it difficult to build prognostic models that hold up across patient populations (Bottner *et al*., 2022). Pinning down the molecular drivers of immunosuppression in HNSCC is therefore central to both prognostic refinement and the rational design of combination immunotherapy regimens.

Cellular senescence has gained increasing attention as a regulator of tumor biology (Casella *et al*., 2019; Sikora *et al*., 2021). Senescent cells are defined in large part by their senescence-associated secretory phenotype (SASP) (Carreno *et al*., 2021; Songkiatisak *et al*., 2022). Early senescence can act as a brake on pre-malignant proliferation, but as senescent cells accumulate within the aging TME, this initially protective response turns counterproductive, fostering immune evasion, angiogenesis and metastatic spread (Huart *et al*., 2022). Integrative multi-omics work has uncovered shared molecular features between aging and cancer across epigenomic, exomic and transcriptomic layers, raising the possibility that senescence-associated programs represent conserved, actionable nodes in tumor progression (Chatsirisupachai *et al*., 2019, 2021; Perez *et al*., 2018).

Age-related molecular differences between younger and older patients further influence checkpoint therapy responses and point to candidate stratification biomarkers (Erbe *et al*., 2021; Shah *et al*., 2021). Against this backdrop, how senescence-associated transcriptional programs interact with anti-tumor immunity and shape therapeutic outcomes in HNSCC has not been systematically examined, and a clinically grounded senescence-based classification for this disease remains missing. Previous studies have reported the prognostic significance of senescence-related tumor microenvironment genes in HNSCC. For example, senescence-associated tumor microenvironment genes have been demonstrated to be associated with patient survival and immune infiltration patterns (Lee *et al*., 2023). However, several important gaps remain. Prior studies primarily focused on predefined gene sets, without systematically comparing the relative biological significance of senescence with other tumor-associated programs, and integrated validation at the single-cell and spatial transcriptomic levels remains lacking.

In this study, seven senescence- and metabolism-related gene sets were screened across 30 TCGA pan-cancer cohorts, and cellular senescence was identified as the feature most consistently associated with clinical outcomes in HNSCC. Starting from senescence-associated differentially expressed genes, a multi-algorithm machine learning framework covering 101 algorithm combinations was applied to construct an RNA-based senescence scoring system, SceScore, anchored by eight genes. SceScore was tested in multiple independent cohorts and showed meaningful associations with overall survival, immune cell composition, checkpoint expression and predicted treatment response. Single-cell and spatial transcriptomic data were then used to trace the origin of the SceScore signal within the HNSCC TME and its distribution across tumor tissue.

Therefore, the present study aimed to systematically characterize senescence-associated molecular programs in HNSCC through a comprehensive multi-omics framework. Specifically, the THEMIS analytical framework was first applied to evaluate the relative biological significance of senescence among multiple tumor-associated biological features. Subsequently, a robust senescence-related prognostic scoring system (SceScore) was established using machine learning algorithms and validated in independent cohorts. Furthermore, the associations between SceScore and prognosis, immune microenvironment remodeling, therapeutic responsiveness and tumor heterogeneity were comprehensively investigated. Finally, single-cell and spatial transcriptomic analyses were performed to validate the cellular and spatial characteristics of senescence-associated molecular programs in HNSCC.

MATERIALS AND METHODS

Dataset collection

RNA-seq data of HNSCC samples and the corresponding clinicopathological information were obtained from The Cancer Genome Atlas (TCGA). The clinicopathological information and whole-genome expression data for GSE42743, GSE65858, and GSE41613 were obtained from the Gene Expression Omnibus (GEO). These three GEO cohorts (GSE42743, GSE65858 and GSE41613) were used exclusively for external prognostic validation of SceScore. The scRNA-seq datasets (GSE181919, GSE195836, GSE139324 and GSE200996) and the spatial transcriptomics dataset (GSE208253) were used for mechanistic and spatial validation analyses and were not included in prognostic performance assessments.

Article in Press

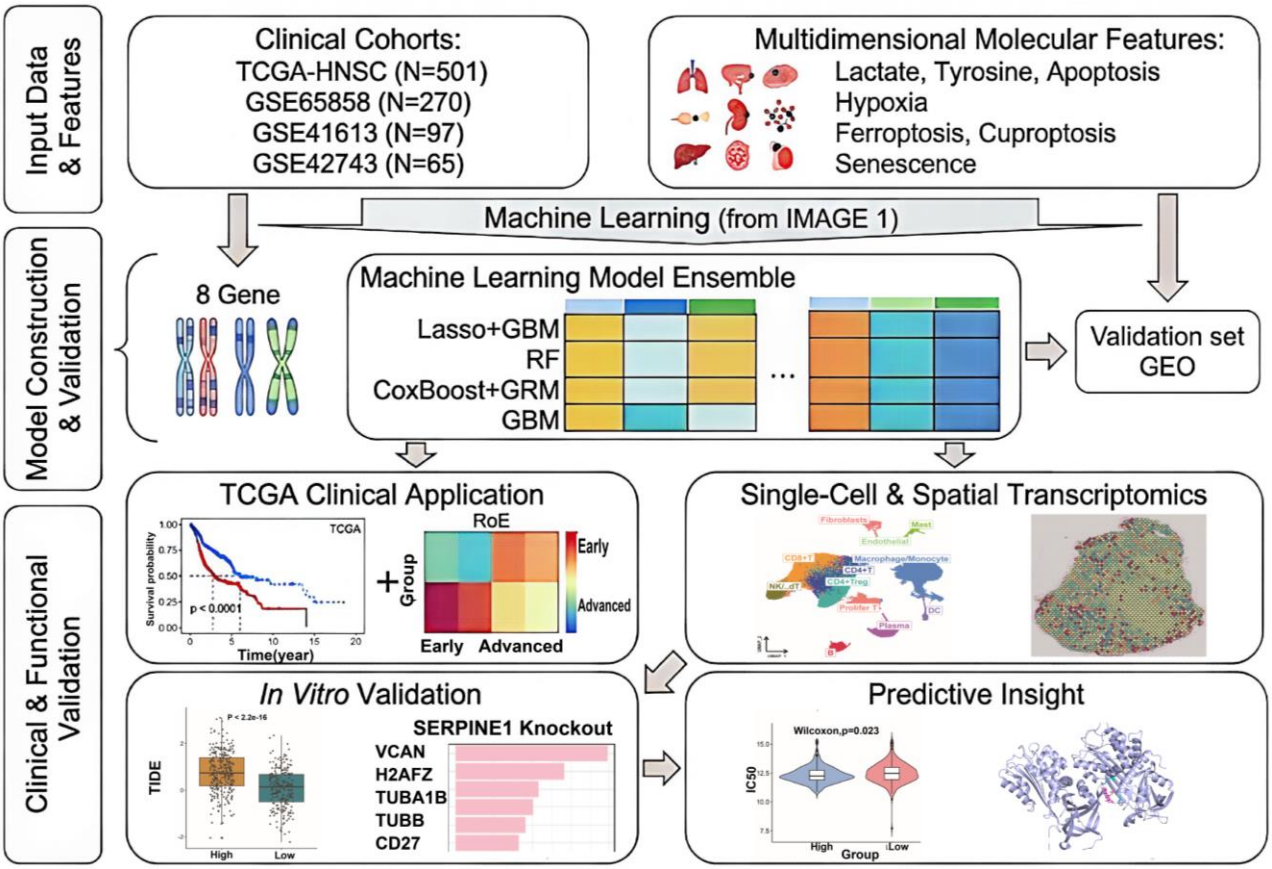


Fig. 1: The scheme of research.

The seven gene signatures associated with distinct biological patterns were Apoptosis, Tyrosine, Hypoxia, Lactate, Ferroptosis, Cuproptosis and Senescence, respectively. After removing duplicates, a total of 669 biological feature genes were included in subsequent analyses. Details are provided in Supplementary Table S1. The overall workflow of the present study is illustrated in Fig. 1.

Molecular subtype identification

Unsupervised consensus clustering of senescence-related genes was using the ConsensusClusterPlus R package (version 1.66.0) to identify potential molecular subtypes. Clustering parameters were set as follows: repetitions (reps) = 50, sample proportion (pItem) = 0.8, feature proportion (pFeature) = 1, with Euclidean distance as the dissimilarity metric (Wilkerson & Hayes, 2010). The same analytical approach was applied to gene sets associated with ferroptosis and lactate metabolism to derive corresponding molecular subtypes. Use the NMF R package (version 0.28) to perform non - negative matrix factorization (NMF) on the TCGA and GEO cohorts. The number of clusters K is gradually increased from 2 to 6 (Gaujoux & Seoighe, 2010). Cluster stability was assessed using the cophenetic correlation coefficient, which plateaued at K = 3; accordingly, K = 3 was selected as the optimal number of clusters. The same NMF framework was subsequently applied to gene sets associated with cuproptosis and tyrosine metabolism under hypoxia conditions to derive the corresponding molecular subtypes.

Differential expression and functional enrichment analysis

The limma R package (version 3.58.1) was used to identify differentially expressed genes (DEGs) between the C3 and C1 senescence subtypes. The screening criteria were as follows: false discovery rate (FDR) < 0.05 and |log2FC| > 1(Ritchie *et al*., 2015). Gene Ontology (GO) enrichment analysis was performed using the clusterProfiler R package (version 4.8.3)(Yu *et al*., 2012). Enrichment significance was assessed by a hypergeometric test, with all RNA-seq-detected genes serving as the background set.

Construction and calculation of SceScore

The SceScore for each HNSCC sample was calculated using the weighted expression values of the signature genes derived from the final prognostic model according to the following formula: SceScore = Σ (βi × Expi), where βi represents the regression coefficient of each signature gene in the final model and Expi represents the normalized expression value of the corresponding gene (Z. Liu *et al*., 2022). The optimal prognostic model was identified through a systematic machine learning benchmarking strategy involving 101 algorithm combinations. Model

Article

robustness and generalizability were evaluated using leave-one-out cross-validation (LOOCV), external validation cohorts, Kaplan–Meier survival analyses, time-dependent ROC analyses and independent prognostic analyses (Table S2). This exhaustive benchmarking strategy was adopted to reduce model-selection bias and systematically identify the most robust prognostic framework across diverse feature-selection and survival-modeling approaches. Importantly, model selection was based on the average C-index across multiple independent external validation cohorts, combined with LOOCV, rather than solely on training-cohort performance, thereby mitigating potential overfitting and improving generalizability.

Independent prognostic validation and nomogram construction

To evaluate SceScore as an independent prognostic factor, univariate and multivariable Cox proportional hazards regression analyses were used, incorporating SceScore alongside relevant clinicopathological variables. Subsequently, prognostic nomograms were developed using the R packages "rms" and "replot" based on the TCGA-HNSC cohort and three GEO cohorts (Z. Zhang & Kattan, 2017). Calibration curves and receiver operating characteristic (ROC) curves are used to evaluate the performance of the nomogram (Alba *et al*., 2017; Chume & Camargo, 2022).

Drug sensitivity prediction

Multiple algorithms, including ESTIMATE and CIBERSORT, were employed to assess the expression of model genes and the levels of various immune cell populations (Sturm *et al*., 2019). The Tumor Immune Dysfunction and Exclusion (TIDE) algorithm (Hao *et al*., 2021) and the "oncoPredict" tool were respectively used to analyze the association between SceScore and responses to immunotherapy and targeted therapy (Maeser *et al*., 2021).

Single-cell RNA sequencing analysis

The Seurat R package (version 4.3.0) was used to analyze scRNA-seq data from the GEO database (GSE181919, GSE195836, GSE139324 and GSE200996) (Hao *et al*., 2021). These procedures included functions such as "PercentageFeatureSet," "SCTransform," "RunPCA," "FindNeighbors," "FindClusters," "RunUMAP," and "FindAllMarkers". Samples with fewer than 500 cells and cells with fewer than 300 detected genes were discarded and the proportion of mitochondrial genes was kept below 15%. Although a 15% mitochondrial gene proportion threshold was applied in the present study to balance data quality and cell retention, applying lower thresholds (e.g., 5–10%) may potentially further reduce the influence of low-quality or dying cells on single-cell analyses and should be considered in future studies. In addition, based on the average expression levels of aging-related genes, the "AddModuleScore" function was used to calculate the specific feature score (SceScore).

Drug repurposing and molecular docking

The Drug Signatures Database (DSigDB) was used to identify potentially effective therapeutic drugs, and the top 10 compounds were selected as candidates based on adjusted p-values (Cai *et al*., 2024). Molecular docking analysis was employed to evaluate the binding affinity of candidate drugs to their targets and assess their druggability (Table S3) (Zaki *et al*., n.d.).

Spatial transcriptomic data processing and SceScore mapping

The raw data of HNSCC were obtained from the GEO database (GSE208253). The aggregated filtered count matrix (HDF5 format) and associated spatial files were imported into R and processed with Seurat (Version 4.3.0) R package. For each sample, spots with fewer than 200 detected features were removed, and the SCTransform function was used to normalize the data and stabilize its variance (D. Ma *et al*., n.d.). After integration, perform dimensionality reduction using principal component analysis (PCA), construct a shared nearest neighbor (SNN) graph and conduct Louvain clustering. Use uniform manifold approximation and projection (UMAP) for two-dimensional visualization and use the SpatialFeaturePlot function to visualize the spatial expression patterns of SceScore-related genes and other markers on tissue sections (Y. Zhang *et al*., 2024).

In-silico gene knockout analysis

To investigate the potential functions of the SceScore-associated network, *in silico gene knockout analysis was performed using the scTenifoldKnk R package* (Osorio *et al*., 2022). The expression matrix of tumor cells was used as input to construct a gene regulatory network and virtual knockouts were simulated for nodes corresponding to SceScore genes. scTenifoldKnk compares the simulated knockout (KO-like) and original (wild-type–like) network states to quantify gene-level perturbation effects and identify differentially regulated genes.

Statistical analysis

All statistical analyses were performed in R (version 4.3.0). Continuous variables are presented as mean +/- standard deviation (SD) or median with interquartile range (IQR) and were compared using Student's t-test or the Wilcoxon rank-sum test. All statistical tests were two-sided and $P < 0.05$ was considered statistically significant unless otherwise specified.

RESULTS

Senescence-based molecular stratification across pan-cancer and HNSCC cohorts

To systematically characterize tumor biology, seven categories of senescence- and metabolism-related biological features were curated—cuproptosis, ferroptosis, cellular senescence, lactate metabolism, hypoxia, apoptosis and tyrosine metabolism—comprising 669

Article in Press

associated genes. Molecular stratification was benchmarked across 30 TCGA pan-cancer datasets and the resulting subtypes were evaluated against eight clinical phenotypes: overall survival (OS), progression-free survival (PFS), mRNA stemness index (mRNAsi), immune infiltration scores (ESTIMATEScore, ImmuneScore and StromalScore) and TIDE (Fig. 2 and Fig. S1-S2). Senescence-related features demonstrated consistent stability and significant clinical relevance across 13 tumor subtypes (Fig. 2a). Using HNSCC as a representative cancer type, senescence features showed the strongest association with clinical phenotypes compared with cuproptosis features (Fig. 2b). Accordingly, unsupervised clustering of senescence-related genes stratified TCGA-HNSC patients into three subtypes: C1, C2 and C3. Kaplan–Meier analysis revealed that C1 patients had significantly better overall survival than those in C2 (P = 0.0099) and C3 (P = 0.0099), while C2 and C3 survival curves partially overlapped at five years (P = 0.715), with C3 showing the worst long-term prognosis (Fig. 2c). Age distribution analysis further demonstrated that C1 had the lowest median age and C3 the highest. Statistical results showed the most significant age difference between C1 and C3 (P = 0.013), with C2 and C3 approaching significance (P = 0.059), whereas no significant difference was observed between C1 and C2 (P = 0.4)(Fig. 2d). Considering both survival and age characteristics, it is believed that C1 represents a low-senescence subtype with favorable prognosis; C3 represents a high-senescence subtype closely associated with advanced age and poor survival outcomes; and C2 exhibits intermediate characteristics.

Differential expression analysis between the C3 and C1 aging subtypes (|log2FC| > 1 and FDR < 0.05) identified 37 aging-related genes that were significantly differentially expressed. In the C3 subtype, 25 genes were upregulated and 12 were downregulated (Fig. 2e). GO enrichment analysis of differentially expressed genes in the C3 subtype revealed significant enrichment in biological processes primarily involving negative regulation of cell proliferation, replicative senescence, cell cycle regulation and apoptosis signaling pathways (Fig. 2f). This supports the rationale for selecting the C3 row as a representative of high senescence. These findings suggest that genes in the C3 subtype may contribute to a poor prognosis by regulating key processes such as cell proliferation, the cell cycle, and apoptosis. Among the 37 differentially expressed genes, univariate Cox regression analysis identified 17 significant risk or protective genes (HR > 1 or HR < 1, P-value < 0.05). A gene network constructed from Spearman correlations revealed correlations among these genes (Fig. 2g). The corresponding forest plot displayed the hazard ratios and significance levels of the 17 genes (Fig. 2h), suggesting that these aging-related genes may contribute to tumor progression.

Developing a prognostic SceScore using integrated machine learning algorithms

In the TCGA-HNSC dataset, 101 predictive models were fitted using a LOOCV framework and further calculated the C-index of each model on validation datasets (Fig. 3a). Interestingly, the optimal model was the Lasso+GBM combination, exhibiting the highest average C-index (0.608) and leading C-index across all validation datasets (Fig. 3a). The optimal λ was obtained when partial bias based on the LOOCV framework reached its minimum in Lasso regression. The 17 genes with non-zero Lasso coefficients were then subjected to GBM, ultimately identifying 8 genes. Subsequently, the expression levels of these 8 genes in the GBM model were used to calculate an aging score for each patient based on their predicted values. The top 8 genes with the highest variable importance were identified (Table 1，Fig. S3). Based on the SceScore values, all patients were stratified into high- and low-SceScore groups. The optimal cutoff value for SceScore stratification was determined using the surv_cutpoint function from the Survminer R package based on maximally selected rank statistics. The corresponding cutoff values for each cohort are provided in the Supplementary Materials.

Heatmaps showed distinct stratification between high and low aging scores in both the TCGA-HNSC training and GSE65858 validation cohorts. Unsupervised hierarchical clustering of senescence-related features effectively divided patients into subgroups, aligning with differences in clinical annotations such as age, stage, and risk (Figs. 3b, c). Across the TCGA-HNSC training dataset and three independent validation cohorts, patients in the high-SceScore group exhibited significantly lower OS compared with the low-SceScore group (all P < 0.05) (Figs. 3d, e; Fig. S4). Pooling all samples confirmed this trend (P < 0.05). Correlation analysis further revealed a significant negative association between SceScore and OS (P < 0.05), with markedly reduced survival observed in patients with high SceScore (Figs. 3f, g). Ro/e (ratio of observed to expected cell numbers) analysis in the TCGA-HNSC cohort indicated that high SceScore was associated with older age, T3–T4 tumors, Stage III–IV disease and the presence of lymph node and distant metastases, whereas low SceScore correlated with younger age, T1–T2 tumors, Stage I–II disease and absence of metastases (Fig. 3h). In the GSE42743 cohort, high SceScore was additionally associated with tumor recurrence (Fig. 3i). Overall, these results indicate that SceScore is significantly associated with clinicopathological characteristics of HNSCC, with high SceScore reflecting a more aggressive tumor phenotype and poorer prognosis.

Article in Press

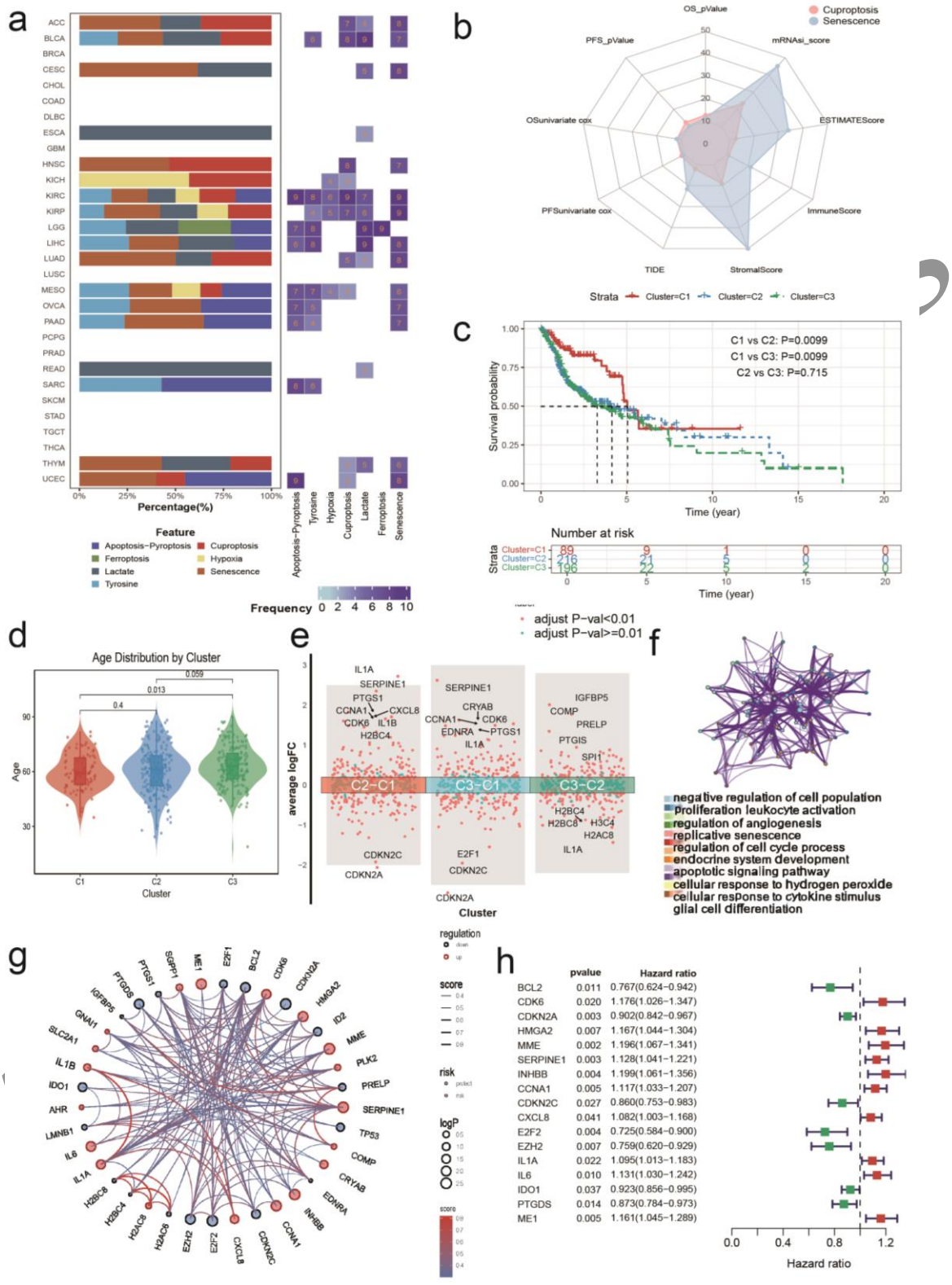


Fig. 2: Pan-cancer comparative analysis identifies senescence features as a superior prognostic framework. (a) Stability heatmap and bar chart across 30 cancer subtypes and seven biological categories; (b) Radar plot comparing senescence and cuproptosis subtypes across eight clinical indicators; (c) Kaplan–Meier overall survival curves; (d) Box-and-whisker plots of age distribution across C1, C2 and C3; (e) Volcano plot; (f) GO analysis; (g) Spearman correlation network of the 17 prognostically significant genes; (h) Forest plot.

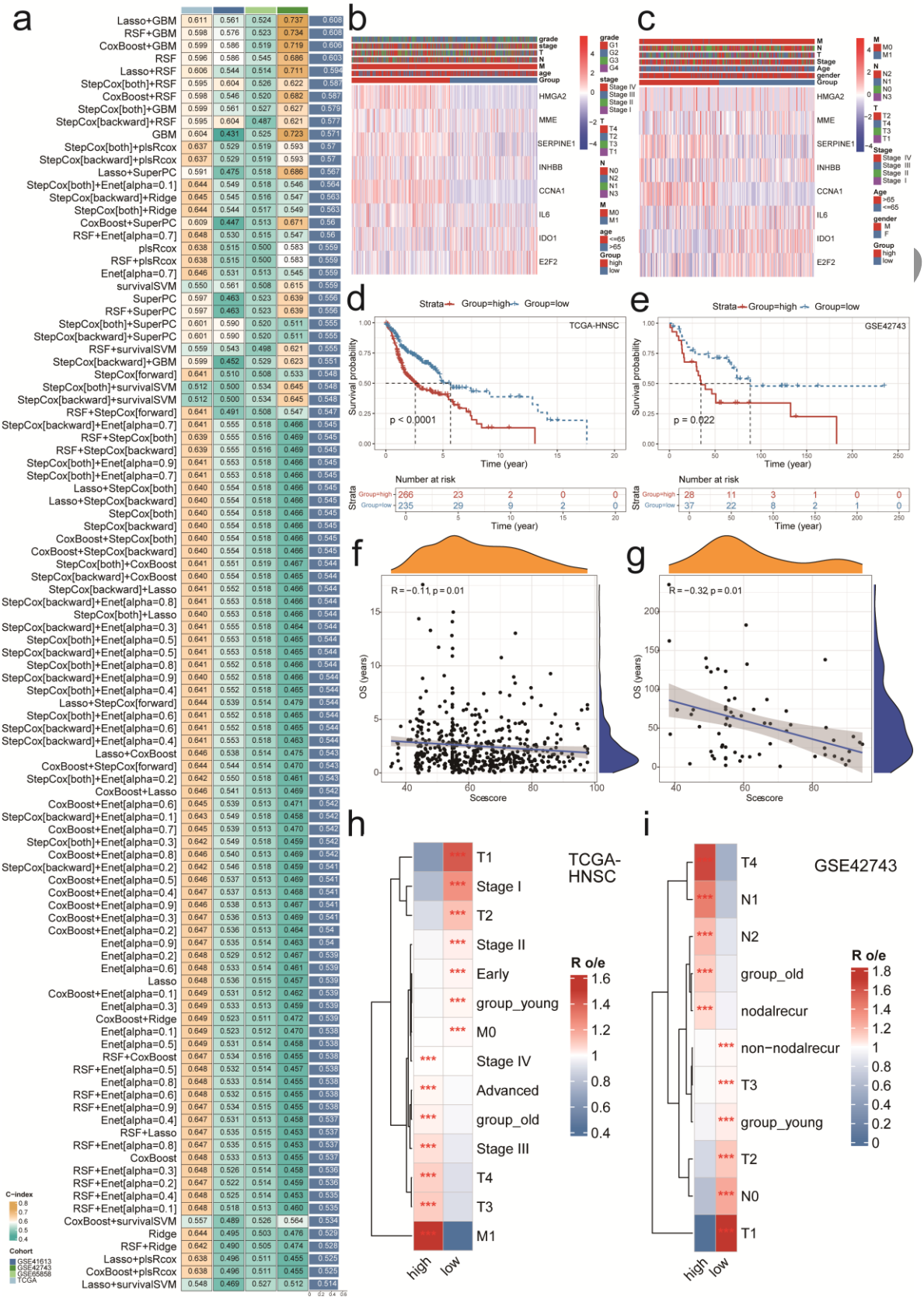


Fig. 3: Construction and validation of the SceScore. (a) C-index values; (b, c) Expression heatmaps; (d, e) Kaplan–Meier overall survival curves; (f, g) Scatter plots; (h, i) Ro/e-based enrichment analysis.

Table 1: Eight SceScore signature genes and their roles in cellular senescence.

Gene	Full Name	Role in senescence / HNSCC
SERPINE1	PAI-1	Classical SASP factor; promotes cell-cycle arrest via p53–p21–Rb axis; linked to immune exclusion and ECM remodeling (Khan *et al*., 2017; Liang *et al*., 2025)
IL6	Interleukin-6	Core SASP inflammatory cytokine; sustains senescent phenotype; drives paracrine senescence and pro-tumorigenic inflammation via JAK-STAT3 (Herbstein *et al*., 2024)
HMGA2	High mobility group A2	Regulates p16INK4a/p19ARF axis; associated with stem cell aging and self-renewal capacity (Nishino *et al*., 2008)
CCNA1	Cyclin A1	Cell-cycle regulator; reflects impaired G1/S transition characteristic of senescent cells (Ji *et al*., 2005)
E2F2	E2F transcription factor 2	Key regulator of E2F–Rb pathway; mediates proliferative arrest during senescence induction (Hayami *et al*., 2010)
IDO1	Indoleamine 2,3-dioxygenase 1	Rate-limiting enzyme in tryptophan metabolism; promotes immune suppression via kynurenine pathway; linked to immunosenescence (Schmidl *et al*., 2025)
INHBB	Inhibin subunit Beta B	TGF-β superfamily member; participates in fibrosis, inflammatory signaling and TME remodeling (Y. Liu, Zhou, *et al*., 2024)
MME	Membrane Metalloendopeptidase (CD10)	Associated with PI3K/AKT-related senescence and TME regulation; marks immunosuppressive CAF subpopulation in HNSCC (Li *et al*., 2021; X.-L. Liu *et al*., 2019)

SceScore delineates an immunosuppressive tumor microenvironment in HNSCC

Compared somatic mutation profiles between high- and low-SceScore groups (Figs. 4a, b). Both groups harbored recurrent alterations in common HNSCC driver genes, including TP53, TTN, PIK3CA, FAT1, SYNE1, LRP1B, CSMD3, NOTCH1, MUC16 and KMT2D. The high-SceScore group had a higher and broader mutational burden (peak ~43 vs 26) and enrichment of TP53 and CDKN2A mutations, whereas the low-SceScore group showed higher frequencies of TTN, PIK3CA, LRP1B (20% vs 14%), NSD1, CASP8 and USH2A. Together, these patterns indicate distinct mutational programs across risk groups; the increased TMB in the high-SceScore group suggests greater genomic instability that may underlie more aggressive tumor biology.To further characterize the immune composition, CIBERSORT was used to quantify 22 immune cell subpopulations. The results indicated that M0 macrophages, Tregs, resting NK cells and resting memory $CD4^+$ T cells were more abundant in high-SceScore tumors. In contrast, activated NK cells, $CD8^+$ T cells and naïve B cells were relatively scarce (Fig. 4c). This pattern is consistent with the hallmarks of an immunosuppressive TME. To elucidate the molecular characteristics underlying risk stratification, the relationship between SceScore and TMB was first assessed; the high-SceScore group showed significantly higher TMB (P = 0.00923; Fig. 4d).

The ESTIMATE algorithm was next applied to assess the tumor immune landscape. Tumors stratified into the high-SceScore group showed notably higher stromal and ESTIMATE scores, along with greater immune cell infiltration and poorer clinical outcomes (Fig. 4e). Beyond immune cell composition, SceScore showed notable correlations with macrophages, dendritic cells and distinct T cell subsets and was also positively associated with the expression of SERPINE1, INHBB, IL-6, HMGA2 and MME (Fig. 4f). In addition, TIDE scores were substantially higher in the high-SceScore group (Fig. 4g), pointing to a greater likelihood of immune evasion and reduced benefit from immunotherapy. In line with this, checkpoint molecules including PD-1 (PDCD1), PD-L1 (CD274), CTLA-4 and IDO1 were more highly expressed in this group, while immune-activating genes tended to be upregulated in low-SceScore tumors (Fig. 4h). These results indicate that elevated SceScore is associated with a pronounced immunosuppressive state, which may have important implications for therapeutic responsiveness.

SceScore is an independent prognostic factor and supports clinical risk nomogram construction

Univariate and multivariate Cox proportional hazards models were further applied to the TCGA - HNSC cohort. In univariate analyses, age (HR = 1.023; 95% CI, 1.009–1.036; P<0.001), M stage (HR = 6.835; 95% CI, 2.508–18.629; P<0.001) and SceScore (HR = 1.017; 95% CI, 1.007–1.026; P<0.001) were significantly associated with overall survival, whereas T stage, overall stage and grade were not (Fig. 5a). In multivariable analysis adjusting for all covariates, age (HR = 1.020; 95% CI, 1.015–1.043; P < 0.001), M stage (HR = 7.862; 95% CI, 2.674–23.109; P < 0.001), N stage (HR = 1.272; 95% CI, 1.022–1.583; P = 0.031) and SceScore (HR = 1.019; 95% CI, 1.009–1.028; P < 0.001) remained independent predictors of overall survival (Fig. 5b).

Article in Press

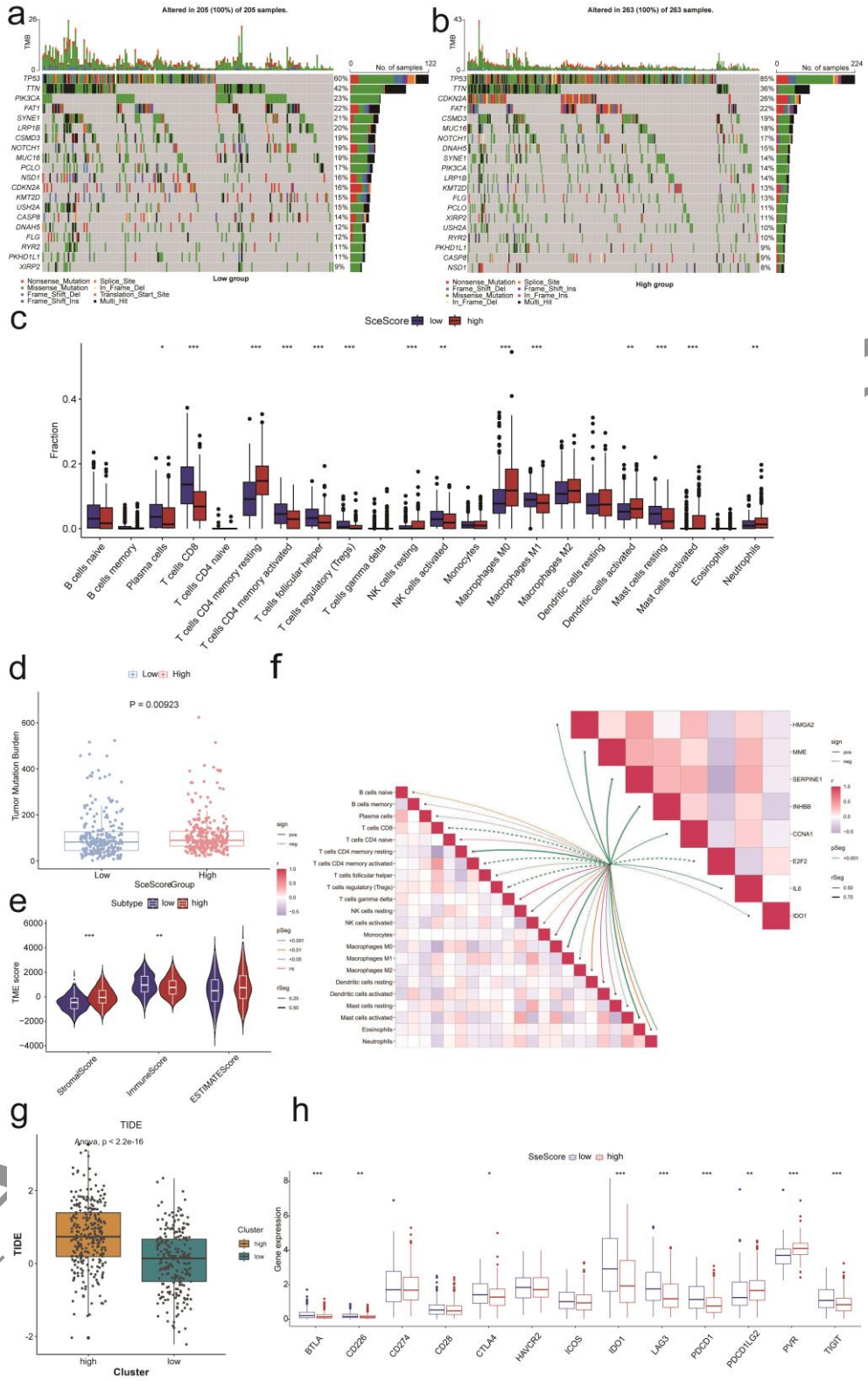


Fig. 4: Relationship between SceScore and the immunosuppressive tumor microenvironment of HNSCC. (a, b) Somatic mutation landscapes; (c) CIBERSORT-inferred; (d) TMB in SceScore groups; (e) ESTIMATE-derived stromal, immune and composite scores by SceScore group; (f) Correlation heatmap between SceScore and immune cell infiltration levels (left) and correlation network of SceScore with key senescence-related genes (right); (g) TIDE scores by SceScore group; (h) Immune checkpoint molecules.

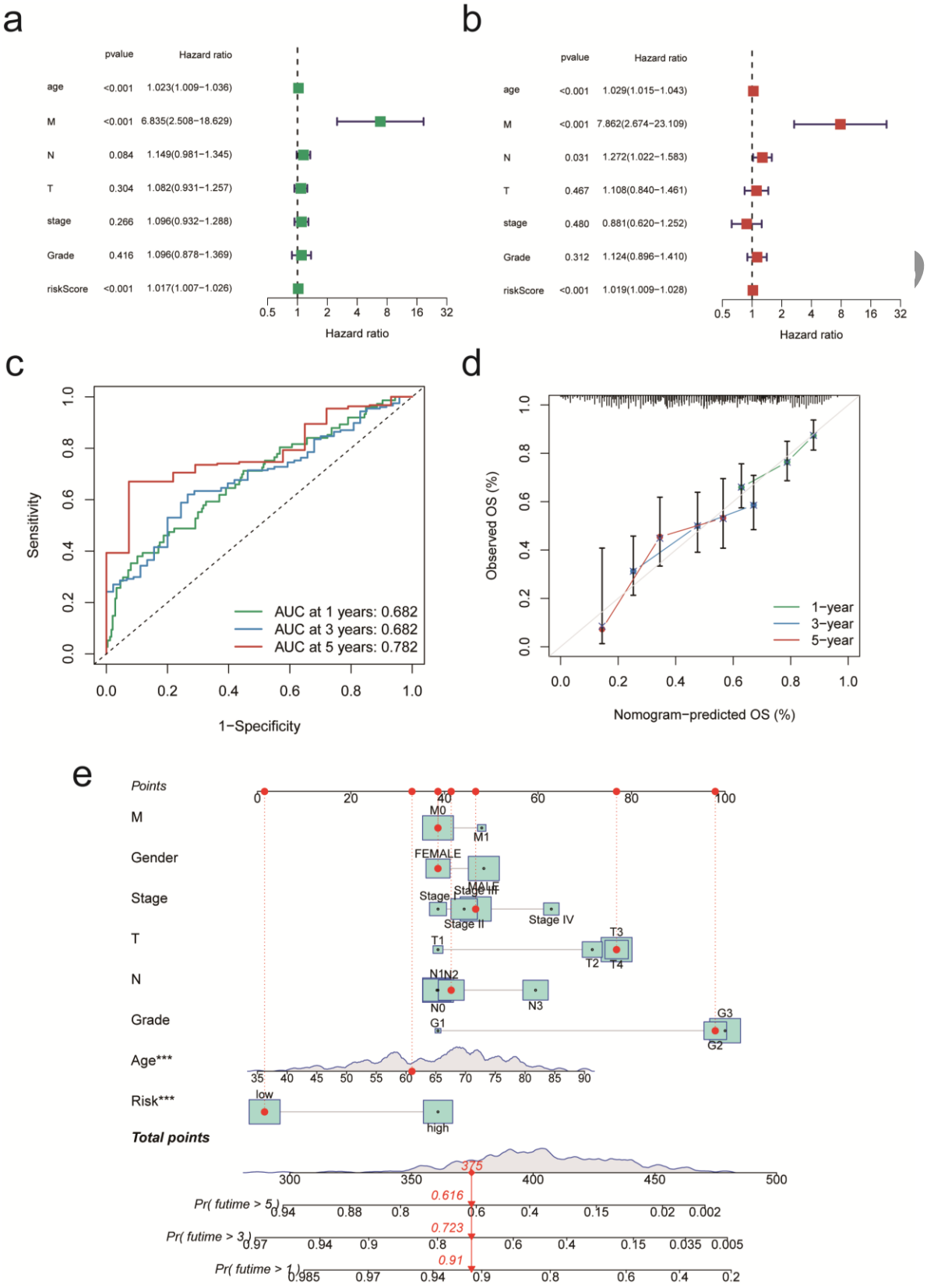


Fig. 5: Validate the nomogram survival model of SceScore. (a) Forest plot of univariate Cox regression analysis; (b) Forest plot of multivariable Cox regression analysis; (c) ROC curves; (d) Calibration plots; (e) Nomogram for individualized survival estimation based on SceScore and clinicopathological variables.

The nomogram assigns a weighted score to each predictor, yielding an individualized risk estimate for patients with HNSCC. Discrimination, assessed by time-dependent ROC curves, showed AUCs of 0.682, 0.682 and 0.782 at 1, 3 and 5 years, respectively (Fig. 5c). Calibration plots comparing predicted probabilities with Kaplan–Meier estimates indicated good agreement across time points (Fig. 5d). On this basis, a prognostic nomogram was constructed. This nomogram combines the SceScore with clinicopathological variables selected by stepwise regression to estimate 1-year, 3-year, and 5-year survival rates (Fig. 5e). External validation in independent cohorts demonstrated comparable AUCs and calibration (Fig. S5), supporting the model's generalizability.

Correlation of SceScore with treatment outcomes in HNSCC patients

To examine how SceScore relates to drug response, half-maximal inhibitory concentrations (IC50) were estimated for multiple agents in HNSCC samples using the GDSC database. Groupwise comparisons confirmed that the high-SceScore group exhibited in carboplatin and gemcitabine and lower in gefitinib, suggesting greater sensitivity to EGFR inhibition (Fig. 6a). These directional associations were further supported by correlation analysis: SceScore correlated positively with carboplatin IC50 ($R = 0.25$, $P = 9.7 \times 10^{\square\square}$) and gemcitabine IC50 ($R = 0.26$, $P = 7.8 \times 10^{\square\square}$) and negatively with gefitinib IC50 ($R = -0.14$, $P = 0.004$) (Figs. 6b–g; Fig. S6). Molecular docking using AutoDock Vina (v1.2.2) was performed for representative target–compound pairs: SERPINE1–spironolactone (predicted $\Delta G = -9.6$ kcal/mol) (Fig. 6h), MME–doxorubicin (−8.3 kcal/mol) (Fig. 6i), IL6–raloxifene (−7.5 kcal/mol) and IDO1–curcumin (−8.0 kcal/mol). Stable binding complexes were characterized by multiple hydrogen bonds and hydrophobic interactions (Table S3). These structure-based results suggest that these compounds may serve as potential modulators of SceScore-related targets and provide a structural basis for subsequent mechanistic and translational investigations. These drug-sensitivity findings are based on in *silico* predictions and should be interpreted as hypothesis-generating computational results. Experimental validation in cell lines and prospective clinical studies are required before these associations can be considered clinically actionable.

Single-cell transcriptomic validation of SceScore cellular origins in the HNSCC tumor microenvironment

To independently validate the immunosuppressive microenvironmental characteristics identified by bulk RNA-seq analysis, the cellular origins of the SceScore signal were interrogated at single-cell resolution. Four publicly available scRNA-seq datasets of HNSCC (GSE181919, GSE195836, GSE139324 and GSE200996) were integrated and, following standard quality control and dimensionality reduction, cells were annotated into malignant epithelial, myeloid, T cell, B cell, cancer-associated fibroblast (CAF) and endothelial populations (Fig. 7a). Using Seurat's AddModuleScore function with the eight-gene signature, an SceScore was computed for each cell and mapped onto a common UMAP embedding. Clear heterogeneity emerged: high-score cells were concentrated in myeloid and CAF compartments, whereas low-score cells were enriched in CD8□ T cells, NK cells and B cells (Fig. 7a). Feature plots confirmed the distribution patterns of SceScore components across the single-cell atlas (Fig. 7b). Individual expression of each gene comprising the SceScore signature was visualized on UMAP plots (Fig. 7c). A chord diagram quantified these relationships, showing tighter connections of the high-score group to myeloid and stromal lineages and of the low-score group to effector/memory T cells and NK cells-consistent with an immunosuppressive, stroma-remodelled high-risk milieu (Fig. 7d). Across the four datasets, three reproducibly showed an association between higher senescence signal and myeloid dominance (Fig. S7 and Fig. S8). Given the prominence of myeloid cells, this compartment was further subclustered into 13 subpopulations, with SceScore recomputed at the subpopulation level (Fig. 7e). Risk-stratified chord analysis revealed selective enrichment of subpopulations 1, 6 and 7 in the high-score group (Fig. 7f). Marker-gene heatmaps indicated that these high-score subpopulations exhibit TAM-like programmes, including SPP1□ and NLRP3□ signatures, suggesting that elevated SceScore is largely driven by tumour-associated macrophage–like myeloid cells (Fig. 7g).

Spatial transcriptomic validation of SceScore distribution and immunosuppressive signaling in tumor tissue

To delineate the spatial distribution of SceScore within tumors and evaluate its biological relevance, three independent spatial transcriptomics datasets were analyzed. Panel shows an H&E-stained section in which tumor regions were delineated by a pathologist (Fig. 8a). Building on the immunosuppressive and stromal-enriched phenotype described above, SceScore activity mapped closely to pathologist-annotated tumor regions, while non-tumor areas showed substantially weaker signal (Fig. 8b). This spatial overlap argues against a stromal or background artifact and instead places the SceScore transcriptional program squarely within the tumor compartment. At the level of individual genes, each SceScore component showed spatially restricted enrichment within distinct microenvironmental niches (Fig. 8c–f), a pattern that held across all three independent spatial datasets examined (Fig. S9 and S10). Strong SceScore signal was not uniformly distributed but instead accumulated preferentially at the tumor periphery forming band-like or patchy zones of enrichment, while the tumor core remained comparatively quiescent.

Article

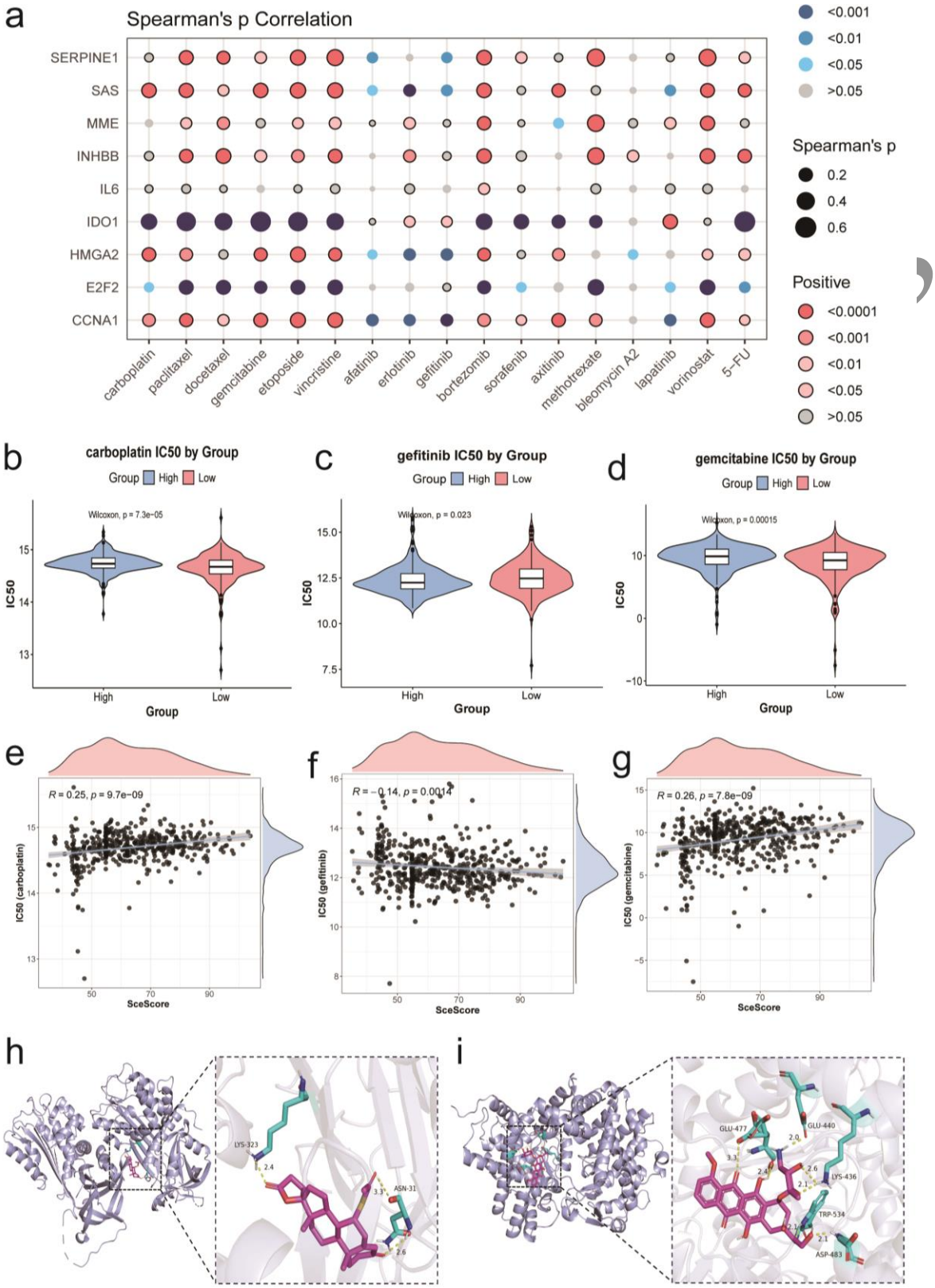


Fig. 6: Association of SceScore with drug sensitivity and molecular docking of candidate therapeutic targets. (a) Spearman correlation matrix of SceScore, senescence-related genes and IC50 values for multiple therapeutic agents; (b–d) IC50 values for carboplatin, gefitinib and gemcitabine; (e–g) Scatter plots; (h) Predicted binding pose of spironolactone in the active site of SERPINE1; (i) Predicted binding pose of doxorubicin in the active site of MME.

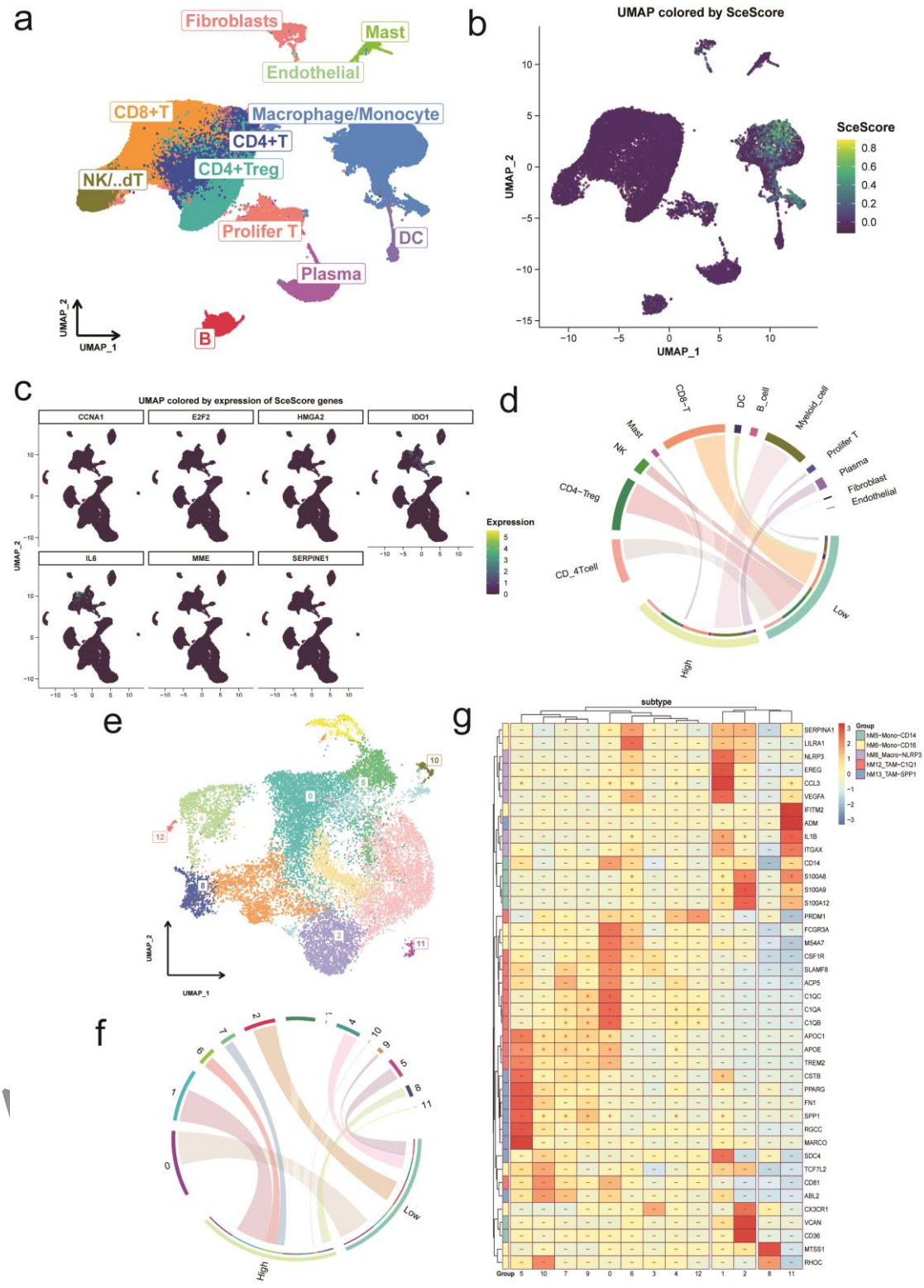


Fig. 7: Single-cell transcriptomic validation of SceScore cellular origins in the HNSCC tumor microenvironment. (a) UMAP of integrated HNSCC scRNA-seq datasets with cell type annotations; (b) UMAP colored by per-cell SceScore; (c) Feature plots of the eight SceScore genes across the single-cell atlas; (d) Chord diagram linking high- and low-SceScore strata to cell-type compartments; (e) UMAP of subclustering within the myeloid compartment; (f) Chord diagram showing enrichment of myeloid subpopulations by SceScore group; (g) Heatmap of marker genes across myeloid subpopulations.

Given that CAFs and myeloid cells are well-established residents of the invasive front, this peripheral bias aligns naturally with the cellular composition inferred from the single-cell data. Within tumor regions, the signal remained heterogeneous and non-uniform, indicating that senescence-associated transcriptional programs are variably activated across spatial niches, reflecting the intratumoral heterogeneity suggested by the bulk-level stratification.

In-silico gene knockout of selected SceScore-related genes using scTenifoldKnk identified downstream differentially expressed genes implicating extracellular matrix remodeling (Fig. 8g), immune regulation and cell-state transitions (Fig. 8h; Fig.S11).Taken together, the spatial validation provides independent, tissue-level evidence that the SceScore-associated transcriptional network reflects a genuine immunosuppressive tumor microenvironment, with biological signals spatially anchored within tumor regions and functionally linked to immune evasion mechanisms identified across all analytical layers.

DISCUSSION

Through systematic evaluation of seven senescence- and metabolism-related biological features across 30 TCGA pan-cancer cohorts, cellular senescence was identified as the most consistently informative feature across multiple key clinical dimensions, including overall survival, progression-free survival, mRNA stemness index, immune infiltration scores and TIDE score. These pan-cancer observations align with and extend prior large-scale integrative analyses demonstrating that aging and cancer share common molecular features across epigenomic, exomic and transcriptomic layers and that senescence-associated programs may participate in tumor initiation and progression through relatively conserved mechanisms across cancer types (D'Ambrosio & Gil, 2023; Xi *et al*., 2024). The directional consistency of these associations across such heterogeneous tumor types suggested that cellular senescence is a potentially generalizable vulnerability, not restricted to any single cancer lineage.

On this basis, the SceScore system was constructed and validated across the TCGA-HNSC training cohort and three independent GEO datasets. In each setting, high SceScore tracked with shorter overall survival and more aggressive clinicopathological features, including advanced T and N stage, older age and lymph node involvement. Multivariable Cox regression confirmed that SceScore retained prognostic value after adjustment for age, T, N, and M stage, suggesting that it captures tumor biology not fully encoded in anatomical staging alone. The present findings are broadly consistent with previous studies highlighting the prognostic and immunological significance of senescence-associated molecular features in HNSCC. (Lee *et al*., 2023) reported that senescence-related tumor microenvironment genes were significantly associated with patient survival and immune infiltration patterns, supporting the concept that cellular senescence contributes to tumor progression and microenvironment remodeling in HNSCC (Lee *et al*., 2023). Similarly, high-SceScore tumors in the present study exhibited significantly worse survival outcomes and distinct immune microenvironment characteristics, including enrichment of immunosuppressive myeloid populations and elevated expression of immune checkpoints. Compared with prior bulk transcriptome-based studies, the present study further integrated single-cell and spatial transcriptomic analyses, identifying SPP1+ tumor-associated macrophages as the principal cellular driver of elevated SceScore, a finding aligned with the established role of SPP1+ macrophages in immune suppression and poor prognosis across solid tumor types.

Embedded in a nomogram alongside standard clinical variables, SceScore yielded AUCs of 0.682, 0.682, and 0.782 at 1, 3, and 5 years, with calibration curves tracking well with Kaplan–Meier estimates across time points. The optimal Lasso + GBM model achieved an average C-index of 0.608, indicating moderate prognostic discriminatory ability. A direct head-to-head comparison with TNM staging alone was not performed in the present study because complete, uniformly recorded staging information was not available across all validation cohorts. Nevertheless, SceScore independently contributed to prognostic estimation in multivariable Cox analysis alongside standard clinicopathological variables including age, T stage, N stage and M stage, suggesting that it captures biological information not fully encoded by anatomical staging alone. Future prospective studies with complete TNM data and matched treatment records would enable a more rigorous evaluation of the incremental prognostic value of SceScore over conventional staging. Compared with previously reported prognostic signatures for HNSCC that were primarily based on single biological themes—such as hypoxia (Toustrup *et al*., 2012), ferroptosis (He *et al*., 2023), or immune-related features (Y. Liu, *et al*., 2024)—the present SceScore model was established following systematic biological feature evaluation using the THEMIS analytical framework, thereby providing a more comprehensive characterization of senescence-associated molecular programs in HNSCC.

The most striking feature of high-SceScore tumors was their immune composition. Rather than the activated, cytotoxic profile associated with checkpoint therapy response, these tumors were populated by M0 macrophages, resting NK cells and Tregs, while CD8 T cells, activated NK cells and plasma cells were correspondingly depleted.

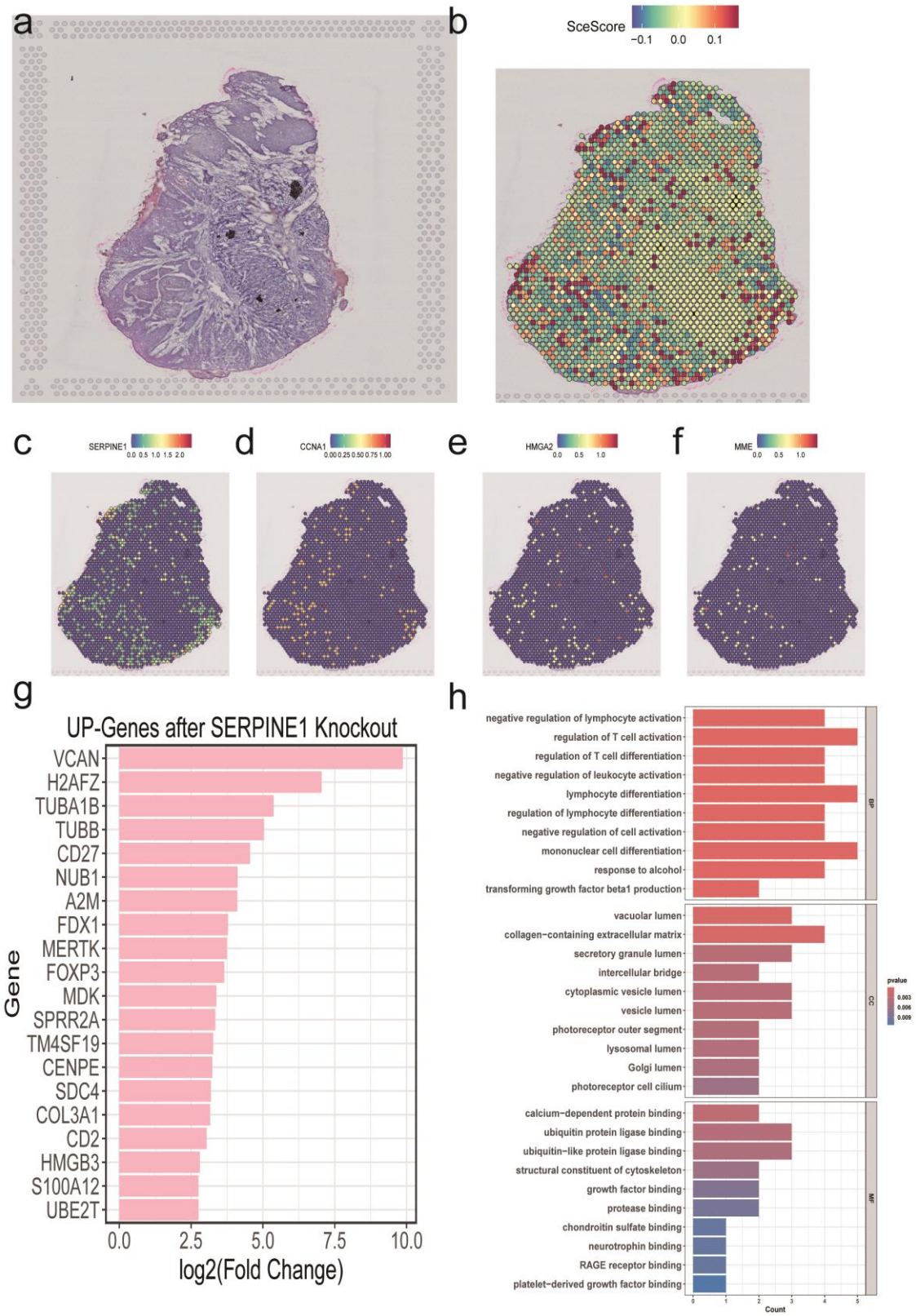


Fig. 8: Spatial transcriptomic validation of SceScore distribution and immunosuppressive signaling in HNSCC tumor tissue. (a) H&E-stained tissue section with pathologist-annotated tumor regions; (b) Spatial distribution of SceScore across the tissue section; (c–f) Spatial expression patterns of SERPINE1, CCNA1, HMGA2 and MME, respectively; (g) Genes expression in silico knockout of SERPINE1; (h) Gene Ontology analysis.

A configuration that resembles the exhausted, immune-excluded TME described in checkpoint-refractory cancers (D. S. Chen & Mellman, 2017; D'Ambrosio & Gil, 2023). Layered on top of this, high-SceScore tumors showed broad upregulation of inhibitory checkpoints (PD-1/PD-L1, CTLA-4, TIGIT, LAG-3, HAVCR2, IDO1 and PVR) and substantially elevated TIDE scores, all pointing toward active immune evasion rather than passive immune absence. This picture aligns with what SASP biology would predict: senescent cells release TGF-β, IL-6, and IL-10, which collectively impair effector T cell activity and skew macrophage polarization toward immunosuppressive states (H. Liu *et al*., 2022; Sun *et al*., 2022). Single-cell data put a cellular face on these bulk observations. Across four integrated HNSCC scRNA-seq datasets, high SceScore signal was concentrated in myeloid cells and CAFs, while low SceScore signal was marked in $CD8^+$ T cells, NK cells, and B cells. Indepth study of the myeloid compartment revealed that three subpopulations characterized by $SPP1^+$ and $NLRP3^+$ are the main sources of high SceScore. $SPP1^+$ macrophages have been repeatedly linked to immunosuppression, matrix remodeling and poor prognosis across solid tumors and NLRP3 inflammasome activation is an established amplifier of SASP and immune evasion (Icer & Gezmen-Karadag, 2018; Wang *et al*., 2025; Wu *et al*., 2022; S. Zhang *et al*., 2023). Taken together, these findings trace a coherent cellular axis: a high senescence burden leads to the dominance of $SPP1^+$/$NLRP3^+$ macrophages, which, in turn, result in an immunosuppressive TME and ultimately poor clinical outcomes.

Several of the eight SceScore genes merit closer attention given their known roles in HNSCC biology. SERPINE1 (PAI-1), which showed the tightest correlation with SceScore and immune infiltration patterns, is a canonical SASP effector that suppresses fibrinolysis, promotes matrix remodeling and has been tied to immune exclusion in multiple tumor types (D. Zhang *et al*., 2024). IDO1 depletes local tryptophan and generates kynurenine metabolites that blunt T cell responses and favor Treg differentiation, making it one of the better-characterized enzymatic mediators of tumor immune evasion (Orecchini *et al*., 2023; Pamart *et al*., 2024). IL-6 drives JAK-STAT3 signaling in both tumor and stromal compartments, fueling pro-tumorigenic inflammation and resistance to apoptosis (R.-J. Ma *et al*., 2022), while MME marks a CAF subpopulation with well-documented immunosuppressive and matrix-remodeling activity in HNSCC (You *et al*., 2022). On the drug-sensitivity side, a high SceScore predicted reduced response to platinum-based agents and gemcitabine, but greater sensitivity to EGFR inhibition—a pattern that may reflect the proliferative and stromal biology captured by the score. Drug repurposing analysis via DSigDB, combined with AutoDock Vina docking, flagged spironolactone (SERPINE1), curcumin (IDO1), raloxifene (IL-6) and doxorubicin (MME) as candidate modulators of SceScore-related targets, with predicted binding affinities ranging from −7.5 to −9.6 kcal/mol. These in silico predictions require experimental validation but offer a starting point for mechanistic work on senescence-targeted interventions in HNSCC. In addition, across three independent datasets, the high-SceScore signal was concentrated within pathologist-defined tumor regions rather than adjacent stroma, ruling out the possibility that the score reflects a background stromal artifact. Within tumor tissue, signal was not evenly spread: it accumulated most prominently along the tumor–stroma interface at the invasive front, forming band-like or patchy zones of enrichment, while the tumor core remained comparatively quiet. This peripheral bias matches the known biology of CAFs and TAM-like cells, which preferentially occupy the invasive front and drive local invasion, lymphovascular spread and adverse prognosis in HNSCC and other solid tumors (Alver *et al*., 2025; Jin *et al*., 2025; Kahlert *et al*., 2011; Sentani *et al*., 2014). The colocalization of high SceScore with this anatomically distinct zone lends tissue-level support to the cellular architecture inferred from single-cell data. *In silico knockout of SERPINE1 and other SceScore genes further implicated extracellular matrix remodeling and immune-regulatory pathways as downstream functional consequences, consistent with the immunosuppressive and stromal remodeling picture that emerged across all analytical layers*.

CONCLUSION

This work brings together pan-cancer molecular stratification, machine-learning–based prognostic modeling, and multi-resolution TME characterization to develop SceScore—a senescence-grounded, independently validated prognostic tool for HNSCC. Beyond its predictive value, SceScore provides a mechanistic window into how senescence programs remodel the immune landscape and sustain disease progression and offers a practical basis for risk stratification, therapy response prediction, and therapeutic target identification. Several caveats apply. The analysis rests entirely on retrospective public datasets; while multi-cohort and multi-omics cross-validation strengthens confidence in the findings, the clinical utility of SceScore will ultimately need to be tested in prospectively collected cohorts with complete treatment records. SceScore was also built solely from transcriptomic data, so its relationship to protein-level expression, epigenetic state, and histopathological features remains untested. Although spatial transcriptomics provided supportive evidence for the enrichment of SPP1+ tumor-associated macrophages in high-SceScore regions, additional immunohistochemistry and immunofluorescence validation using independent clinical samples will be necessary to confirm the spatial localization and biological significance of these findings. Additionally, the consensus clustering iteration count (reps = 50) and the mitochondrial gene proportion threshold (15%) represent methodological choices that future studies may wish to optimize.

Acknowledgements
The authors are grateful to the Cancer Genome Atlas (TCGA), Gene Expression Omnibus (GEO), UCSC Xena, cBioPortal, ArrayExpress, the National Center for Biotechnology Information (NCBI), the Genomics of Drug Sensitivity in Cancer (GDSC) database, and the pioneering researchers who provided the datasets.

Author's contributions
Miaomiao Lu: Methodology; Formal analysis; Writing—original draft. Yue Xi: Methodology; Writing—review and editing. Yan Chen: Formal analysis. Xinyu Liu: Formal analysis; Data curation. Ruiyu Guo: Data curation. Qingqing Wan: Data curation. Xin Zou: Methodology; Investigation. Wantao Chen: Conceptualization; Writing—review and editing. All authors read and approved the final manuscript.

Funding
This work was supported by grants from the National Natural Science Foundation of China [32570782 to X.Z.], the Shanghai Jiao Tong University Trans-med Awards Research (Grant No. 20250203).

Data availability statement
All data analyzed during this study are publicly available from the following repositories: Bulk RNA-seq data and clinicopathological information for HNSCC were obtained from The Cancer Genome Atlas (TCGA; https://portal.gdc.cancer.gov/); gene expression data for validation cohorts (GSE42743, GSE65858, GSE41613), single-cell RNA sequencing datasets (GSE181919, GSE195836, GSE139324, GSE200996) and spatial transcriptomics data (GSE208253) were obtained from the Gene Expression Omnibus (GEO; https://www.ncbi.nlm.nih.gov/geo/). Drug sensitivity data were obtained from the Genomics of Drug Sensitivity in Cancer (GDSC) database (https://www.cancerrxgene.org/). No new primary data were generated in this study."

Ethical approval
Ethical approval was not required for this study because all analyses were based exclusively on publicly available and de-identified datasets from The Cancer Genome Atlas (TCGA) and the Gene Expression Omnibus (GEO). No human participants were directly recruited, and no identifiable human data or biological samples were collected in this study. This study was performed in adherence with the STROBE guidelines. See supplementary file for the STROBE checklist.

Conflict of interest
The authors declare that they have no competing interests.

REFERENCES

Alba AC, Agoritsas T, Walsh M, Hanna S, Iorio A, Devereaux PJ, McGinn T and Guyatt G (2017). Discrimination and calibration of clinical prediction models: Users' guides to the medical literature. *JAMA*, **318**(14): 1377–1384.

Alver TN, Bergholtz H, Holm MB, Dorg LT, Skrede ML, Kure EH and Verbeke CS (2025). Spatial transcriptomics reveals cancer and stromal cell heterogeneity between center and invasive front of pancreatic cancer. *Mod Pathol*, **38**(6): 100726.

Bottner J, Ribbat-Idel J, Klapper L, Jagomast T, Lemster AL, Perner S, Idel C and Kirfel J (2022). Elevated LSD1 and SNAIL Expression indicate poor prognosis in hypopharynx carcinoma. *Int J Mol Sci*, **23**(9): 5075.

Cai X, Xu F, Wang Z, Chen H and Lin S (2024). Prognostic biomarkers for hepatocellular carcinoma based on serine and glycine metabolism-related genes. *J Clin Transl Hepatol* , **12**(3): 266–277.

Carreno G, Guiho R and Martinez-Barbera JP (2021). Cell senescence in neuropathology: A focus on neurodegeneration and tumours. *Neuropathol Appl Neurobiol* , **47**(3): 359–378.

Casella G, Munk R, Kim KM, Piao Y, De S, Abdelmohsen K and Gorospe M (2019). Transcriptome signature of cellular senescence. *Nucleic Acids Res*, **47**(14): 7294–7305.

Chatsirisupachai K, Lesluyes T, Paraoan L, Van Loo P and de Magalhães JP (2021). An integrative analysis of the age-associated multi-omic landscape across cancers. *Nat Commun*, **12**(1): 2345.

Chatsirisupachai K, Palmer D, Ferreira S and de Magalhães JP (2019). A human tissue-specific transcriptomic analysis reveals a complex relationship between aging, cancer and cellular senescence. *Aging Cell*, **18**(6): e13041.

Chaves P, Garrido M, Oliver J, Pérez-Ruiz E, Barragan I and Rueda-Domínguez A (2023). Preclinical models in head and neck squamous cell carcinoma. *Br J Cancer*, **128**(10): 1819–1827.

Chen DS and Mellman I (2017). Elements of cancer immunity and the cancer-immune set point. *Nature*, **541**(7637): 321–330.

Chen H, Yang Y, Deng Y, Wei F, Zhao Q, Liu Y, Liu Z, Yu B and Huang Z (2022). Delivery of CD47 blocker SIRPα-Fc by CAR-T cells enhances antitumor efficacy. *J Immunother Cancer*, **10**(2): e003737.

Chow LQM (2020). Head and Neck Cancer. *N Engl J Med*, **382**(1): 60–72.

Chume FC and Camargo JL (2022). ROC curves: Stats, common sense and caution. *Endocrine*, **76**(2): 506–507.

D'Ambrosio M and Gil J (2023). Reshaping of the tumor microenvironment by cellular senescence: An opportunity for senotherapies. *Dev Cell*, **58**(12): 1007–1021.

Erbe R, Wang Z, Wu S, Xiu J, Zaidi N, La J, Tuck D, Fillmore N, Giraldo NA, Topper M, Baylin S, Lippman M, Isaacs C, Basho R, Serebriiskii I, Lenz HJ, Astsaturov I, Marshall J, Taverna J, Lee J, Jaffee EM, Roussos Torres ET, Weeraratna A, Easwaran H and Fertig EJ (2021). Evaluating the impact of age on

Article in Press

immune checkpoint therapy biomarkers. *Cell Rep*, **36**(8): 109599.

Ferris RL, Blumenschein G Jr, Fayette J, Guigay J, Colevas AD, Licitra L, Harrington KJ, Kasper S, Vokes EE, Even C, Worden F, Saba NF, Iglesias Docampo LC, Haddad R, Rordorf T, Kiyota N, Tahara M, Lynch M, Jayaprakash V, Li L and Gillison ML (2018). Nivolumab vs investigator's choice in recurrent or metastatic squamous cell carcinoma of the head and neck: 2-year long-term survival update of CheckMate 141 with analyses by tumor PD-L1 expression. *Oral Oncol*, **81**: 45–51.

Ferris RL, Blumenschein G Jr, Fayette J, Guigay J, Colevas AD, Licitra L, Harrington K, Kasper S, Vokes EE, Even C, Worden F, Saba NF, Iglesias Docampo LC, Haddad R, Rordorf T, Kiyota N, Tahara M, Monga M, Lynch M, Geese WJ, Kopit J, Shaw JW and Gillison ML (2016). Nivolumab for recurrent squamous-cell carcinoma of the head and neck. *N Engl J Med*, **375**(19): 1856–1867.

Gaujoux R and Seoighe C (2010). A flexible R package for nonnegative matrix factorization. *BMC Bioinformatics,* **11**(1): 367.

Gigot M, Digonnet A, Rodriguez A and Lechien JR (2022). Salvage Partial Laryngectomy after failed radiotherapy: Oncological and functional outcomes. *J Clin Med*, **11**(18): 5411.

Hao Y, Hao S, Andersen-Nissen E, Mauck WM 3rd, Zheng S, Butler A, Lee MJ, Wilk AJ, Darby C, Zager M, Hoffman P, Stoeckius M, Papalexi E, Mimitou EP, Jain J, Srivastava A, Stuart T, Fleming LM, Yeung B, Rogers AJ, McElrath JM, Blish CA, Gottardo R, Smibert P and Satija R (2021). Integrated analysis of multimodal single-cell data. *Cell*, **184**(13): 3573-3587.e29.

Hayami S, Yoshimatsu M, Veerakumarasivam A, Unoki M, Iwai Y, Tsunoda T, Field HI, Kelly JD, Neal DE, Yamaue H, Ponder BAJ, Nakamura Y and Hamamoto R (2010). Overexpression of the JmjC histone demethylase KDM5B in human carcinogenesis: Involvement in the proliferation of cancer cells through the E2F/RB pathway. *Mol Cancer*, *9*: 59.

He R, Zhang X, Wu Y, Weng Z and Li L (2023). TTC7B is a new prognostic biomarker in head and neck squamous cell carcinoma linked to immune infiltration and ferroptosis. *Cancer Med*, **12**(24): 22354–22369.

Herbstein F, Sapochnik M, Attorresi A, Pollak C, Senin S, Gonilski-Pacin D, Ciancio Del Giudice N, Fiz M, Elguero B, Fuertes M, Muller L, Theodoropoulou M, Pontel LB and Arzt E (2024). The SASP factor IL-6 sustains cell-autonomous senescent cells via a cGAS-STING-NFκB intracrine senescent noncanonical pathway. *Aging Cell*, **23**(10): e14258.

Huart C, Fransolet M, Demazy C, Le Calvé B, Lucas S, Michiels C and Wéra A-C (2022). Taking advantage of the senescence-promoting effect of olaparib after X-ray and proton irradiation using the senolytic drug, ABT-263. *Cancers*, **14**(6): 1460.

Icer MA and Gezmen-Karadag M (2018). The multiple functions and mechanisms of osteopontin. *Clin Biochem*, **59**: 17–24.

Ji P, Agrawal S, Diederichs S, Baumer N, Becker A, Cauvet T, Kowski S, Beger C, Welte K, Berdel WE, Serve H and Müller-Tidow C (2005). Cyclin A1, the alternative A-type cyclin, contributes to G1/S cell cycle progression in somatic cells. *Oncogene*, **24**(16): 2739–2744.

Jin W, Yu Q, Yu L, Zhou T, Wang X, Lu W, Zhang X, Ding L, Hu Q and Ni Y (2025). HAS1high cancer associated fibroblasts located at the tumor invasion front zone promote oral squamous cell carcinoma invasion via ECM remodeling. *J Exp Clin Cancer Res*, **44**(1): 238.

Kahlert C, Lahes S, Radhakrishnan P, Dutta S, Mogler C, Herpel E, Brand K, Steinert G, Schneider M, Mollenhauer M, Reissfelder C, Klupp F, Fritzmann J, Wunder C, Benner A, Kloor M, Huth C, Contin P, Ulrich A and Weitz J (2011). Overexpression of ZEB2 at the invasion front of colorectal cancer is an independent prognostic marker and regulates tumor invasion in vitro. *Clin Cancer Res*, **17**(24): 7654–7663.

Khan SS, Shah SJ, Klyachko E, Baldridge AS, Eren M, Place AT, Aviv A, Puterman E, Lloyd-Jones DM, Heiman M, Miyata T, Gupta S, Shapiro AD and Vaughan DE (2017). A null mutation in SERPINE1 protects against biological aging in humans. *Sci Adv*, **3**(11): eaao1617.

Lee YC, Nam Y, Kim M, Kim SI, Lee J-W, Eun Y-G and Kim D (2023). Prognostic significance of senescence-related tumor microenvironment genes in head and neck squamous cell carcinoma. *Aging*, **16**(2): 985–1001.

Li Q, Wang Y, Xu L, Wang L, Guo Y and Guo C (2021). High level of CD10 expression is associated with poor overall survival in patients with head and neck cancer. *Int J Oral Maxillofac Surg*, **50**(7): 857–864.

Liang X, Zhang J, Yu J, Zhao J and Yang S (2025). Quercetin ameliorates ox-LDL-induced cellular senescence of aortic endothelial cells and macrophages by p16/p21, p53/SERPINE1 and AMPK/mTOR pathways. *Eur J Med Res*, **30**(1): 359.

Liu H, Zhao D, Li H, Zhang W, Lin Q, Wang X, Zheng S, Zhang L, Li L, Hu S and Hu Y (2022). Blocking iASPP/Nrf2/M-CSF axis improves anti-cancer effect of chemotherapy-induced senescence by attenuating M2 polarization. *Cell Death Dis*, **13**(2): 166.

Liu X-L, Liu J-L, Xu Y-C, Zhang X, Wang Y-X, Qing L-H, Guo W, Ding J and Meng L-H (2019). Membrane metallo-endopeptidase mediates cellular senescence induced by oncogenic PIK3CAH1047R accompanied with pro-tumorigenic secretome. *Int J Cancer*, **145**(3): 817–829.

Liu Y, Lin H, Zhong W, Zeng Y, Zhou G, Chen Z, Huang S, Zhang L and Liu X (2024). Multi-omics analysis of immune-related microbiome and prognostic model in head and neck squamous cell carcinoma. *Clin Oral Investig*, **28**(5): 263.

Liu Y, Zhou Q, Zou G and Zhang W (2024). Inhibin subunit beta B (INHBB): An emerging role in tumor

Article in Press

progression. *J Physiol Biochem*, **80**(4): 775–793.
Liu Z, Liu L, Weng S, Guo C, Dang Q, Xu H, Wang L, Lu T, Zhang Y, Sun Z and Han X (2022). Machine learning-based integration develops an immune-derived lncRNA signature for improving outcomes in colorectal cancer. *Nat Commun*, **13**(1): 816.
Ma D, Herndon N, Le JQ, Abruzzi KC, Zinn K and Rosbash M (2023). Neural connectivity molecules best identify the heterogeneous clock and dopaminergic cell types in the Drosophila adult brain. *Sci Adv*, **9**(8): eade8500.
Ma R-J, Zheng Q-M, Zhang N and Sun Z-G (2022). Clinicopathological Significance of STAT3 and p-STAT3 among 91 patients with adenocarcinoma of the esophagogastric junction. *Dis Markers*, *2022*: 9311684.
Maeser D, Gruener RF and Huang RS (2021). oncoPredict: An R package for predicting in vivo or cancer patient drug response and biomarkers from cell line screening data. *Brief Bioinform*, **22**(6): bbab260.
Nishino J, Kim I, Chada K and Morrison SJ (2008). Hmga2 promotes neural stem cell self-renewal in young but not old mice by reducing p16Ink4a and p19Arf expression. *Cell*, **135**(2): 227–239.
Orecchini E, Belladonna M, Pallotta M, Volpi C, Zizi L, Panfili E, Gargaro M, Fallarino F, Rossini S, Suvieri C, Macchiarulo A, Bicciato S, Mondanelli G and Orabona C (2023). The signaling function of IDO1 incites the malignant progression of mouse B16 melanoma. *Oncoimmunology*, **12**(1): 2170095.
Osorio D, Zhong Y, Li G, Xu Q, Yang Y, Tian Y, Chapkin RS, Huang JZ and Cai JJ (2022). scTenifoldKnk: An efficient virtual knockout tool for gene function predictions via single-cell gene regulatory network perturbation. *Patterns*, **3**(3): 100434.
Pamart G, Gosset P, Le Rouzic O, Pichavant M and Poulain-Godefroy O (2024). Kynurenine Pathway in Respiratory Diseases. *Int J Tryptophan Res,* **17**: 11786469241232871.
Pérez RF, Tejedor JR, Bayón GF, Fernández AF and Fraga MF (2018). Distinct chromatin signatures of DNA hypomethylation in aging and cancer. *Aging Cell*, **17**(3): e12744.
Ritchie ME, Phipson B, Wu D, Hu Y, Law CW, Shi W and Smyth GK (2015). Limma powers differential expression analyses for RNA-sequencing and microarray studies. *Nucleic Acids Res*, **43**(7): e47.
Schmidl B, Lauterbach M, Stögbauer F, Mogler C, Ribbat-Idel J, Perner S and Wollenberg B (2025). Immunohistochemical Profiling of IDO1 and IL4I1 in Head and Neck Squamous Cell Carcinoma: Interplay for Metabolic Reprogramming? *Int J Mol Sci*, **26**(8): 3719.
Seiwert TY, Burtness B, Mehra R, Weiss J, Berger R, Eder JP, Heath K, McClanahan T, Lunceford J, Gause C, Cheng JD and Chow LQ (2016). Safety and clinical activity of pembrolizumab for treatment of recurrent or metastatic squamous cell carcinoma of the head and neck (KEYNOTE-012): An open-label, multicentre, phase 1b trial. *Lancet Oncol*, **17**(7): 956–965.
Sentani K, Matsuda M, Oue N, Uraoka N, Naito Y, Sakamoto N and Yasui W (2014). Clinicopathological significance of MMP-7, laminin γ2 and EGFR expression at the invasive front of gastric carcinoma. *Gastric Cancer*, **17**(3): 412–422.
Shah Y, Verma A, Marderstein AR, White J, Bhinder B, Garcia Medina JS and Elemento O (2021). Pan-cancer analysis reveals molecular patterns associated with age. *Cell Rep*, **37**(10): 110100.
Sikora E, Bielak-Zmijewska A and Mosieniak G (2021). A common signature of cellular senescence; does it exist? *Ageing Res Rev*, *71*: 101458.
Songkiatisak P, Rahman SMT, Aqdas M and Sung M-H (2022). NF-κB, a culprit of both inflamm-ageing and declining immunity? *Immun Ageing*, *19*: 20.
Sturm G, Finotello F, Petitprez F, Zhang JD, Baumbach J, Fridman WH, List M and Aneichyk T (2019). Comprehensive evaluation of transcriptome-based cell-type quantification methods for immuno-oncology. *Bioinformatics*, **35**(14): i436–i445.
Sun J, Park C, Guenthner N, Gurley S, Zhang L, Lubben B, Adebayo O, Bash H, Chen Y, Maksimos M, Muz B and Azab AK (2022). Tumor-associated macrophages in multiple myeloma: Advances in biology and therapy. *J Immunother Cancer*, **10**(4): e003975.
Sung H, Ferlay J, Siegel RL, Laversanne M, Soerjomataram I, Jemal A and Bray F (2021). Global Cancer Statistics 2020: GLOBOCAN Estimates of Incidence and Mortality Worldwide for 36 Cancers in 185 Countries. *CA Cancer J Clin*, **71**(3): 209–249.
Toustrup K, Sørensen BS, Alsner J and Overgaard J (2012). Hypoxia gene expression signatures as prognostic and predictive markers in head and neck radiotherapy. *Semin Radiat Oncol*, **22**(2): 119–127.
Wang H, Gao Y-C, Ming-Zhang, Dai G-C, Lu P-P, Li Y-J, Cao M-M, Liu X-Y, Sheng R-W, Shi L, Zhang C, Cui W-G and Rui Y-F (2026). Quercetin attenuates tendon stem/progenitor cell senescence and promotes aged tendon repair via AKT/NF-κB/NLRP3-mediated mitophagy activation. *J Adv Res*, **83**: 741–758.
Wilkerson MD and Hayes DN (2010). ConsensusClusterPlus: A class discovery tool with confidence assessments and item tracking. *Bioinformatics*, **26**(12): 1572–1573.
Wu Y, Yang S, Ma J, Chen Z, Song G, Rao D, Cheng Y, Huang S, Liu Y, Jiang S, Liu J, Huang X, Wang X, Qiu S, Xu J, Xi R, Bai F, Zhou J, Fan J, Gao Q (2022). Spatiotemporal immune landscape of colorectal cancer liver metastasis at single-cell level. *Cancer Discovery*, **12**(1): 134–153.
Xi Y, Zheng K, Deng F, Liu Y, Sun H, Zheng Y, Tong HHY, Ji Y, Zhang Y, Chen W, Zhang Y, Zou X and Hao J (2024). Themis: Advancing precision oncology through comprehensive molecular subtyping and optimization. *Briefings Bioinform*, **25**(4): bbae261.
Yang S, Wang Y, Jia J, Fang Y, Yang Y, Yuan W and Hu J

Article in Press

(2024). Advances in engineered macrophages: A new frontier in cancer immunotherapy. *Cell Death Dis*, **15**(4): 238.

You Y, Tian Z, Du Z, Wu K, Xu G, Dai M, Wang Y and Xiao M (2022). M1-like tumor-associated macrophages cascade a mesenchymal/stem-like phenotype of oral squamous cell carcinoma via the IL6/Stat3/THBS1 feedback loop. *J Exp Clin Cancer Res*, *CR*, **41**(1): 10.

Yu G, Wang L-G, Han Y and He Q-Y (2012). clusterProfiler: An R package for comparing biological themes among gene clusters. *Omics*, **16**(5): 284–287.

Zaki I, Moustafa AMY, Beshay BY, Masoud RE, Elbastawesy MAI, Abourehab MAS and Zakaria MY (2022). Design and synthesis of new trimethoxylphenyl-linked combretastatin analogues loaded on diamond nanoparticles as a panel for ameliorated solubility and antiproliferative activity. *J Enzyme Inhib Med Chem*, **37**(1): 2679–2701.

Zhang C, Li Z, Zhang Y, Zhao C, Wang H, Lin J, Liu C, Wang X and Wang H (2022). Genomic variations and immune-related features of TMB, PD-L1 expression and CD8+ T Cell infiltration in chinese pulmonary sarcomatoid carcinoma. *Int J Gen Med*, **15**: 4209–4220.

Zhang D, Zhang J-W, Xu H, Chen X, Gao Y, Jiang H-G, Wang Y, Wu H, Yang L, Wang W-B, Dai J, Xia L, Peng J and Zhou F-X (2024). Therapy-induced senescent tumor cell-derived extracellular vesicles promote colorectal cancer progression through SERPINE1-mediated NF-κB p65 nuclear translocation. *Mol Cancer*, **23**(1): 70.

Zhang S, Peng W, Wang H, Xiang X, Ye L, Wei X, Wang Z, Xue Q, Chen L, Su Y and Zhou Q (2023). C1q+ tumor-associated macrophages contribute to immunosuppression through fatty acid metabolic reprogramming in malignant pleural effusion. *J Immunother Cancer*, **11**(8): e007441.

Zhang Y, Chen S, Xu L, Chu S, Yan X, Lin L, Wen J, Zheng B, Chen S and Li Q (2024). Transcription factor PagMYB31 positively regulates cambium activity and negatively regulates xylem development in poplar. *The Plant Cell*, **36**(5): 1806–1828.

Zhang Z and Kattan MW (2017). Drawing Nomograms with R: Applications to categorical outcome and survival data. *Ann Transl Med*, **5**(10): 211.

Article in Press